Radiochim. Acta **95**, 439–450 (2007) / **DOI** 10.1524/ract.2007.95.8.439

Synthesis and characterization of the solid uranium(VI) dioxo-diacetohydroxamate complex

By C.-M. S. Gong, F. Poineau and K. R. Czerwinski*

Nuclear Sciences and Technology Division, Harry Reid Center for Environmental Studies, University of Nevada, Las Vegas, 4505 Maryland Parkway, NV 89154-4009, USA

(Received January 7, 2007; accepted in revised form February 13, 2007)

UREX / Acetohydroxamic acid / Uranium / NMR / XAFS / Infrared spectroscopy

Summary. A novel dry synthesis for the uranium(VI) dioxo-diacetohydroxamate (UAHA) complex has been developed. The complex was generated in > 80% yield by mechanically grinding solid uranyl acetate dihydrate (UAc) with solid acetohydroxamic acid in stoichiometric amounts. The resulting $UO_2(AHA)_2 \cdot 4H_2O$ solid is purified by washing with acetone. The stoichiometry was confirmed *via* colorimetric assays for U(VI) and AHA. The analogous ferric trisacetohydroxamate complex (FeAHA) was synthesized for comparison.

The UAHA solid was extensively characterized by ultraviolet-visible (UV-vis), Fourier-transform infrared (FT-IR), and extended X-ray absorption fine structure (EXAFS) spectroscopies. The compound did not fluoresce after laser excitation. Proton nuclear magnetic resonance (NMR) spectra were obtained of the complex in D_2O, acidified acetonitrile-d_3, and DMSO-d_6. The solubility was determined over a range of solvents. It was determined that in the purified solid, two bidentate AHA molecules bind to uranyl *via* the carbonyl and hydroxamate oxygen atoms, a structure analogous to known ferric, nickel, and lanthanum AHA complexes. In an acidic environment, binding is monodentate through the hydroxamate oxygen. And in aqueous solution, the UAHA complex assumes both binding moieties, depending on the pH. This pH-dependent speciation change is demonstrated for the first time.

The easy synthesis and purification of UAHA enables researchers to strictly control reaction conditions; to eliminate interfering salts and water; and to study the complex in the solid-phase.

1. Introduction

Acetohydroxamic acid (AHA) is an organic reductant under consideration for use in the proposed UREX separations process [1, 2]. Various hydroxamic acids have been shown to preferentially complex tetravalent over hexavalent actinides [3–6]. Acetohydroxamic acid selectively reduces Np(VI) and Pu(IV) without reducing U(VI), enabling the separation of uranium during solvent extraction [7–12]. The uranyl-AHA complex forms easily in aqueous solution, but is largely dissociated; aqueous stability constants have been reported in aqueous media as $\log k_1 = 7.63$ and $\log k_2 = 6.62$ ($\log \beta_2 = 14.25$) in 0.15 M NaCl [13] and $\log \beta_1 = 8.22$ and $\log \beta_2 = 15.30$ in 0.1 M KNO_3 [14]. However, the UAHA complex has not been systematically characterized, and no literature on the solid complex is available.

In determining the stability constants above, the models assumed that AHA acts as an O,O bidentate ligand in aqueous complexes with actinides, similar to the siderophore-actinide [15–20], and lanthanide- and transition metal-AHA complexes [21–30]. However, work performed in this laboratory and elsewhere [31, 32] has shown that the maxima of the aqueous UV-vis spectra are dependent on pH, but the spectrum will reach an equilibrium as the pH increases. This could indicate an increased number of bound ligands as free AHA is deprotonated; however, it is shown in this paper that if the pH is held at or below 5.0 at a constant ionic strength, the shape of the UV-vis spectrum does not change to match the high pH spectrum, even at thousandfold excess AHA, and the absorbance continues to increase with increasing ligand. The disparity between the spectra obtained *via* pH and AHA titrations indicate a significant speciation change with pH, such as a conformational difference in U-AHA binding or the formation of a mixed-hydroxide species. Comparison of the UV-vis spectrum of the solid to the aqueous spectra helps to elucidate the geometry of the aqueous complexation.

Recent explorations into the nature of AHA have indicated that its rotational isomeric composition is pH- and solvent-dependent; that the ligand is overwhelmingly in the *Z*-conformation; and that protonation stabilizes the *E* isomer [33–40]. The reported pK_a of acetohydroxamic acid at 25 °C varies from 8.7–9.46 [41–43] and changes according to temperature [44]. An increasing body of literature confirms theoretical calculations that AHA is preferentially an N-acid, stabilized by resonance, tautomerization, and isomeric conformation [45, 46]. The different isomers and anions raise the intriguing possibility of complexation *via* the nitrogen as well as the oxygen atoms. Infrared spectroscopy can confirm the presence of an N−H bond, and the assignments can be correlated to those of the known FeAHA complex [47]. Thus the O,O or O,N geometry can be confirmed in the solid phase, whereas in solution the strong water O−H absorption overwhelms the ligand signals, and

*Author for correspondence (E-mail: czerwin2@unlv.nevada.edu).

the high degree of dissociation makes it difficult to discriminate between free and bound ligand.

Solution-phase ^{1}H NMR in D_2O can demonstrate a change in the complexation with pH by monitoring the methyl peak and correlating the changes to the UV-vis spectra. The NMR spectra of UAHA in DMSO-d_6 can be compared to those of the starting material and FeAHA analogue to observe exchangeable protons. We demonstrate using ^{1}H-NMR that there are at least two binding moieties for aqueous UAHA, and that the distribution between them is pH dependent; that in DMSO, the solid has only one binding geometry; and that the speciation can be correlated to the changes in the UV-vis spectra.

Because it dissociates, the aqueous solubility of the UAHA complex depends on the relative AHA concentration and pH. Higher ligand concentration prevents the formation of insoluble uranyl hydroxide, as does high acid concentrations, which also limits complexation [31]. However, the UAHA solubility in other solvents has remained unexplored because of the unavailability of UAHA solid. The formation constants reported in the literature indicate that the complex is more stable than a number of uranyl salts, such as uranyl nitrate ($\log\beta_1 = -0.30$ to -1.4; $\log\beta_2 = -1.6$ to -1.4) [48] and uranyl acetate ($\log\beta_1 = 2.58$; $\log\beta_2 = 4.37$; $\log\beta_3 = 6.86$) [49]. Therefore the formation of UAHA from either of these starting materials is thermodynamically favored, and only the activation energy needs to be overcome. Evaporation of the aqueous complex yields a precipitate mixed with the counterion salts, unreacted starting material, and uranyl and AHA hydrolysis products. The high-yielding solid-state synthesis described here largely circumvents these problems: it avoids the aqueous decomposition of AHA, which is dependent on the concentration of free ligand, radiation levels, and acid concentration [50–52]; it avoids the hydrolysis of uranyl [48, 53–56]; and the acetic acid byproduct can be cleanly removed with unreacted starting materials with a thorough acetone wash.

2. Experimental

2.1 Chemicals and instruments

Acetohydroxamic acid (Alfa Aesar), uranyl nitrate hexahydrate (International Bio-Analytical Industries, Inc.), and UAc (The General Chemical Company) were powdered separately. Ferric chloride hexahydrate, reagent-grade sodium hydrogen carbonate, sodium perchlorate, nonaqueous dissolution assay solvents (except acetone), boron nitride, Arsenazo(III), benzophenone, and anthroquinone were obtained from Sigma-Aldrich; spectroscopic grade KBr from International Crystal Labs; uranyl standards from Inorganic Ventures; HPLC grade acetone, perchloric acid, and nitric acid from JT Baker; deuterated solvents from Cambridge Isotope Labs; pH standards from Thermo-Orion; and ammonium acetate from EMD Chemicals. Water was purified with a Millipore system. All gases were obtained from Praxair.

UV-vis spectroscopy was performed on a Cary 6000i dual-beam spectrometer and a Cary 50 spectrometer and microplate reader. Liquids were measured at room temperature in 1 cm PMMA cuvettes (VWR brand) or Corning UV-transparent microplates using the chemical matrix as a reference. The FT-IR spectra were measured from 500 to 4000 cm^{-1} under continuous dry nitrogen flow using a Varian Excalibur spectrometer with a KBr beamsplitter. Attenuated total reflectance infrared (ATR-FT-IR) spectra were obtained using an integrated DuraSampler diamond-ATR. For NMR, 400 MHz NMR tubes from Wilmad Labglass were used. Uranyl solutions were further contained in capped Teflon inserts from New-Era Spectro. A Varian 400-NMR spectrometer was used and spectra averaged using the VNMRJ software. Scanned spectra were converted to comma separated values format using the UN-SCAN-IT software from Silk Scientific. Laser fluorescence samples were excited with a 414 nm Optotek laser and monitored from 420 to 780 nm with a Princeton Instruments integrated spectrometer. For pH titrations, a Brinkmann Micro pH electrode was 4-point calibrated with Thermo-Orion standards.

2.2 Synthesis and purification

Powdered samples of 0.390 g UAc and 0.158 g AHA were manually ground together in an agate mortar until a sticky, dark orange paste was formed, after 15 min of vigorous grinding. This was washed three times in cold acetone by batch resuspension and dried under gentle vacuum overnight for a final yield of 0.382 g (89%).

Alternative methods of energy input were explored. Stoichiometric amounts of powdered UAc and AHA were mixed well for good contact, then a) pressed between two tungsten carbide anvils for ten minutes under vacuum and 148, 296, and 591 MPa of pressure; or b) mixed and heated to 60 °C for 5, 15, and 60 min. The products were washed twice with cold acetone by batch resuspension, then dried to a golden orange powder.

Uranyl nitrate was examined as an alternative starting material. A sample of 0.258 g (0.55 mmol) uranyl nitrate and 0.080 g (1.07 mmol) AHA were mixed *via* vortexing in a plastic screw-cap tube and formed a dense, red-purple liquid upon contact. This product was significantly more difficult to isolate and purify due to the HNO_3 byproduct, which enhances UAHA solubility in acetone and other organic solvents, and this synthetic route was not pursued further.

To test the synthesis method, FeAHA was obtained by mixing 1.051 g of finely ground $FeCl_3 \cdot 6H_2O$ (3.89 mmol) with 0.8340 g (11.12 mmol) AHA in a plastic tube. One mL of acetone was added to aid mixing, then 0.9330 g (3 equiv.) solid $NaHCO_3$ added to neutralize the HCl byproduct. The water and acetone were evaporated off. The resulting brown powder was dissolved in hot ethanol and filtered to remove the NaCl. The filtrate was dried to form a dark red powder. For comparison, FeAHA was synthesized according to literature [23]. The purity of all products was assessed *via* UV-vis, ^{1}H-NMR, and ATR-FT-IR spectroscopies.

2.3 Chemical analysis

2.3.1 Stoichiometry

Three independent UAHA samples were dissolved in water. Aliquots of each were diluted volumetrically in 0.1 N HNO_3 and the [U] measured using the Arsenazo method [58]. In the inverse of a reported Fe(III) assay [59], the concentration

of AHA was measured by mixing 100 μL of sample with 800 μL 1 mM $FeCl_3$ and monitoring the 500 nm FeAHA peak. Freshly prepared aqueous AHA solutions, whose concentrations were verified *via* potentiometric endpoint titration, and 1 : 2 mixtures of uranyl and AHA standard solutions were used for calibration. Solutions with uranyl concentrations up to 10 mM did not interfere with the Fe assay; solutions of AHA up to 5 mM did not interfere with the Arsenazo assay.

2.3.2 Solubility

The UAHA final product and UAc starting material were dissolved to saturation in various nonaqueous solvents, centrifuged to remove residual material, the supernatant pushed through a 0.2 μm filter where possible, and replicates prepared. The U and AHA concentrations were measured colorimetrically; for calibration, U and AHA standards were mixed in a 1 : 2 molar ratio.

The solubility of AHA in acetone was measured by dissolving AHA to saturation at 18 °C. The suspension was centrifuged to remove solids and four aliquots were measured into pre-weighed glass vials. The solutions were allowed to evaporate and the resulting crystalline residue was weighed.

2.3.3 Thermal decomposition

A Mel-Temp 1001D melting point apparatus with a 0–400 °C Hg thermometer was used. Melting point standards (47–49 and 283–285 °C) melted within 1 degree of certified values.

2.4 Spectroscopic characterization

2.4.1 UV-vis

Dried UAHA was mixed into KBr at 2 wt. % and dried again. The resulting powder was milled again and pressed at 630 MPa of pressure under vacuum. The resulting transparent orange pellet was placed in a cardboard holder and coated with Nujol oil to retard moisture clouding. A spectrum of Nujol demonstrated its transparency at the relevant wavelengths.

For the AHA titrations, samples were prepared to 0.1, 0.2, and 1 mM uranyl and up to 7000 molar excess AHA. The pH was adjusted to 2.0, 4.0, or 5.0 and the ionic strength to 0.1 or 1.0 M with $NaClO_4$. For the pH titrations, 1 mM uranyl perchlorate with 10 or 20 mM AHA in a sodium perchlorate matrix was thoroughly purged with UHP Ar gas before and during the experiment. The pH was adjusted with 1 M Ar-purged NaOH and aliquots were sampled for UV-vis analysis.

2.4.2 FT-IR

KBr pellets of UAc, AHA, and UAHA and D_2O-exchanged AHA and UAHA were prepared as above. FeAHA and unpurified reaction products were characterized *via* ATR-FTIR.

2.4.3 NMR

AHA, UAHA, and FeAHA were dissolved to saturation in the NMR solvents listed in Table 5. Acetonitrile-d_3 was acidified to dissolve the UAHA. After NMR analysis, the samples were diluted as necessary and the UV-vis spectra measured in microplates.

2.4.4 EXAFS

The unpurified product was milled with boron nitride to 1.8 wt. % uranium, packed into a solid polycarbonate cavity, and sealed with 0.7 mil Kapton tape. Uranium L^{III} edge (17 166 eV) X-Ray absorption spectra were collected at the Advanced Photon Source Basic Energy Science Synchrotron Research Center (APS-BESSRC-CAT) station 12BM using a Si (1,1,1) double crystal monochromator. Spectra were recorded in fluorescence using a 13 element germanium detector. Energy calibration was done using an Yttrium foil (K edge = 17 038 eV).

EXAFS spectra were recorded between k [0–15] $Å^{-1}$ and averaged. The background contribution was removed using AUTOBK software and data analysis was performed using WINXAS. For the fitting procedure, amplitude and phase shift function were calculated by FEFF8.2. The feff.input files were generated by ATOMS using crystallographic structures of uranyl acetate.

2.4.5 Laser fluorescence

The UAc, UAHA, and AHA solids were packed into borosilicate glass capillaries and examined for fluorescence at room temperature.

3. Results

3.1 Synthesis and purification

The various methods are summarized in Table 1. The progression of the reaction was monitored *via* ATR FT-IR by the loss of the intrabonded hydroxamate O−H stretches [60] and the appearance of the acetic acid byproduct O−H [61]. The recovery is the percentage of the total mass recovered after purification with acetone. The yield is based on complete conversion of UAc to UAHA. The recovery decreases with decreasing efficiency, since unreacted starting materials are removed during purification.

Table 1. Synthesis methods, recoveries, and yields.

Method	Recovery[a]	Yield[b]
Milled – 1 equiv. AHA	98%	42%
Milled – 2 equiv. AHA	88%	84%
Milled – 3 equiv. AHA	72%	83%
Milled – 4 equiv. AHA	65%	91%
Milled – 5 equiv. AHA	58%	89%
60 °C, 5 min	84%	18%
60 °C, 15 min	73%	81%
60 °C, 60 min	99%	92%
Pressure, 149 MPa	81%	44%
Pressure, 296 MPa	81%	57%
Pressure, 591 MPa	82%	63%

a: Percentage of starting material total mass recovered;
b: Percentage of theoretical mass of $UO_2(AHA)_2 \cdot 4H_2O$ recovered after purification with acetone.

The best results were obtained by manual grinding with two equivalents of AHA. The reaction was negligible at less than 4 tons (296 MPa) of pressure or 15 min of heat. After sixty minutes of mild heat, the reaction was nearly complete with no loss of mass, but displayed AHA breakdown products in the IR signature.

The starting materials are soluble in acetone, and the product is not, which enables the purification. Attempts to precipitate UAHA from starting material solutions in acetone were unsuccessful – the starting materials simply precipitated out separately. Precipitation from aqueous solutions yielded a wet orange material. Its FT-IR spectrum was identical to that of the solid-state product, but this synthetic route is far less efficient, as the majority of the uranium remained in the mother liquor. The iron analogue was obtained in 95% yield and its purity verified by spectroscopy and comparison to literature [47].

3.2 Chemical characterization

3.2.1 Stoichiometry

The stoichiometry was confirmed by colorimetric measurements. The Arsenazo calibration curve was linear from 0 to 500 μM uranyl, and the novel Fe-AHA assay was linear from 1 to 25 mM AHA (Fig. 1). The R^2 value for each calibration line was > 0.995. The concentrations for the independently prepared solutions are given in Table 2, showing a stoichiometry of $UO_2(AHA)_2$. Two samples were thoroughly dried to exclude loosely bound water, then tested as above. Using mass balance, these samples yielded the formulae $UO_2(AHA)_{1.7}\cdot 4.3H_2O$ and $UO_2(AHA)_{1.9}\cdot 4.7H_2O$. The general formula is extrapolated from this and EXAFS to $UO_2(AHA)_{1.9\pm0.1}\cdot 4H_2O \pm 1H_2O$.

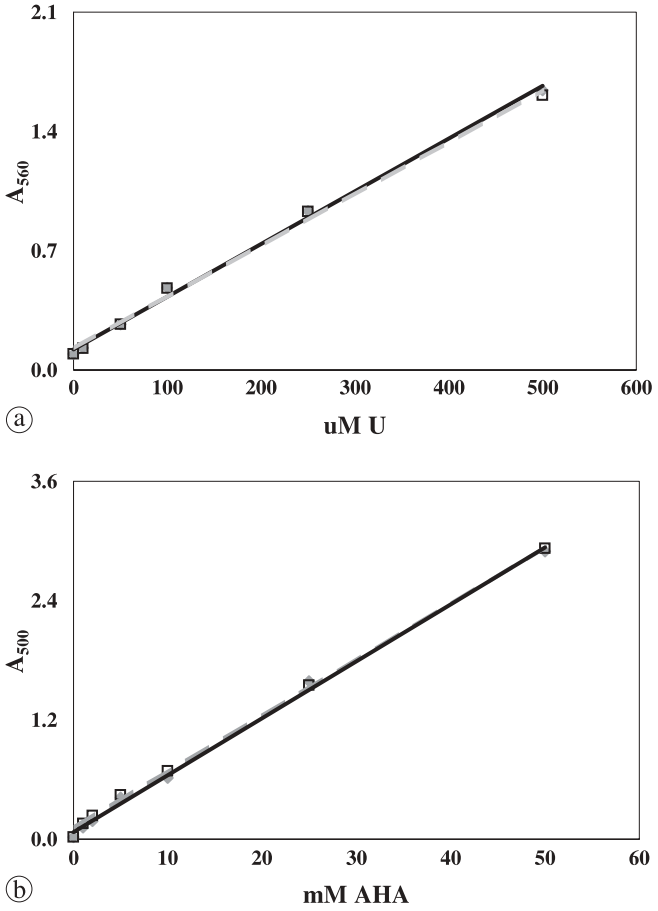

Fig. 1. (**a**) Calibration of Arsenazo(III) mixture to uranyl standards *via* absorbance at 650 nm. Closed, without AHA; open, with two molar equivalents of AHA. (**b**) Calibration of Fe(III) detection method for AHA *via* absorbance at 500 nm. Closed, without uranyl; open, with half molar equivalent of uranyl.

Table 2. Stoichiometry of independent solutions.

Sol.	Mass (mg)	Vol. (mL)	[U] (mM)[a]	[AHA] (mM)[b]	[AHA]/[U]
1	7.4	10	1.43 ± 0.05	2.66 ± 0.20	1.86
2	21.0	100	0.47 ± 0.05	0.84 ± 0.10	2.00
3	29.1	10	5.31 ± 0.10	9.67 ± 0.25	1.81
4	Sat.[c]	2	14.41 ± 0.30	27.92 ± 0.75	1.94
5[d]	5.5	10	1.24 ± 0.04	2.10 ± 0.08	1.72
6[d]	5.9	25	0.38 ± 0.04	0.73 ± 0.08	1.91

a: Determined by Arsenazo(III) assay;
b: Determined by Fe(III) assay;
c: saturated at 18 °C and filtered at 0.45 μm;
d: Dried at 105 °C for 5 days.

3.2.2 Solubility

The solubility of AHA in acetone was measured at 41.81 ± 0.27 g/L (0.56 M) and that of UAc at 4.09 ± 0.07 g/L (11.5 mM). Uranyl-AHA is insoluble in the nonpolar solvents examined. Table 3 demonstrates the relation of uranyl-AHA solubility to dielectric constant. The solubility in water is likely limited by uranyl hydrolysis, and the aqueous UV-vis spectrum resembles that of uranyl hydroxide.

3.2.3 Thermal decomposition

The UAHA product appeared to decompose to a gray ash between 260–280 °C; UAc, which has been reported

Table 3. Solubility in various solvents.

Solvent	Dielectric constant	[U][a] (mM)
Dodecane	2.0	n.d.[b]
Hexane	2.02	n.d.
Benzene	2.28	n.d.
Diethyl ether	4.34	n.d.
30% TBP in dodecane		n.d.
Toluene	5.1	n.d.
Chloroform	5.5	n.d.
Ethyl acetate	6.02	n.d.
Tetrahydrofuran	7.52	n.d.
Tributylphosphate (TBP)	7.8	n.d.
Dichloromethane	9.08	n.d.
Water/TBP	10.0	n.d.
Acetone	20.7	n.d.
Ethanol	24.3	n.d.
Methanol	33.0	n.d.
Acetonitrile	36.6	n.d.
Dimethylformamide	38.3	n.d.
Dimethylsulfoxide	47.2	24.8
Water	80	6.4

a: Determined by Arsenazo(III) assay at 18 °C;
b: not detectable, < 50 μM.

to begin to decompose at 200–245 °C and complete by 297–400 °C [62, 63], had clearly decomposed to a brown residue by 300 °C.

3.3 Spectroscopic characterization

3.3.1 UV-vis

The aqueous UV-vis spectra depend on pH rather than on stoichiometry (Fig. 2). At low pH, the spectrum demonstrates the UAHA maxima at 374 and 476 nm. The spectrum begins to shift above pH 4.0 and is completely transformed by pH 7.9. No maximum could be found for the higher pH spectrum using derivatives. Some slight uranyl hydroxide character is observed at lower AHA concentrations at circumneutral pH, but is not discernable when the AHA is in 30 times or greater molar excess. Under acidic conditions, even at very large excess AHA, the peak shape remains the same; the pH-dependent change in spectrum is therefore not likely to be due to increased AHA coordination, but rather a change in complexation mode.

Fig. 3 illustrates the change in the UV-vis spectrum with ionic strength and pH. Fig. 3a shows that the absorbance of a 1 mM uranyl solution at pH 4 increases with increas-

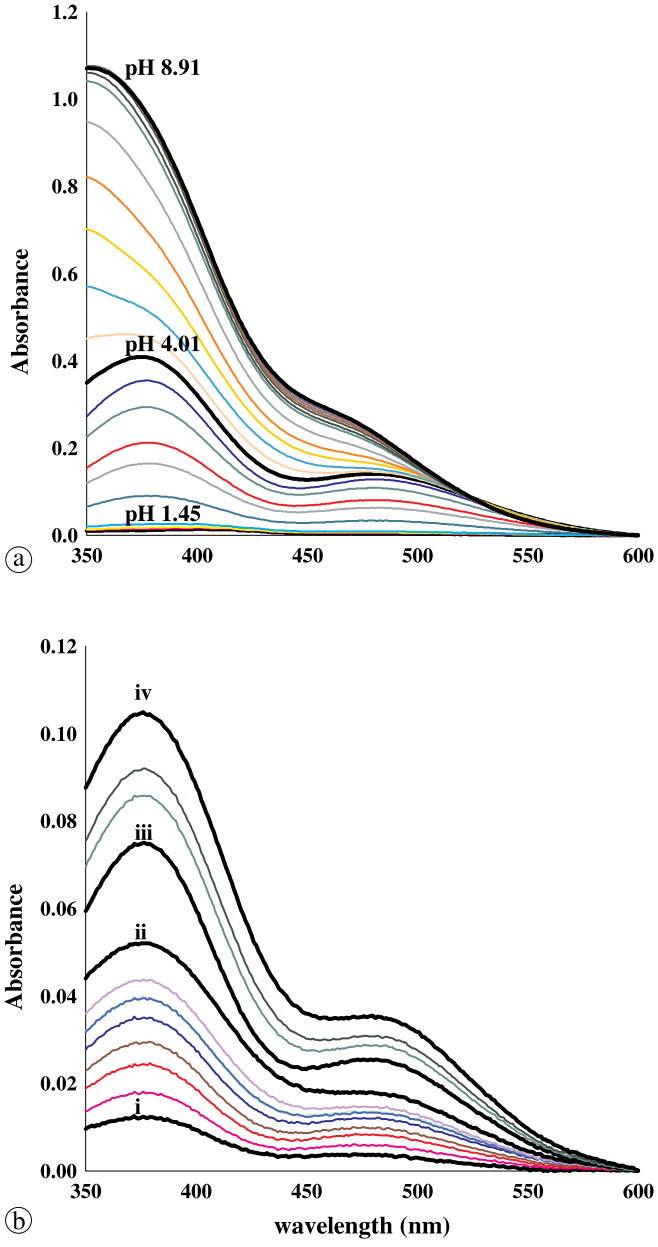

Fig. 2. (**a**) Effect of pH on the UV-vis spectrum of an aqueous solution of 1 mM uranyl, 20 mM AHA, and 1 M ionic strength (NaClO4). Thicker lines correspond to the stated pH. (**b**) AHA titration at pH 4.0. i. 0.1 mM U, 10 mM AHA; ii. 0.1 mM U, 700 mM AHA; iii. 0.2 mM U, 200 mM AHA; iv. 0.2 mM U, 800 mM AHA.

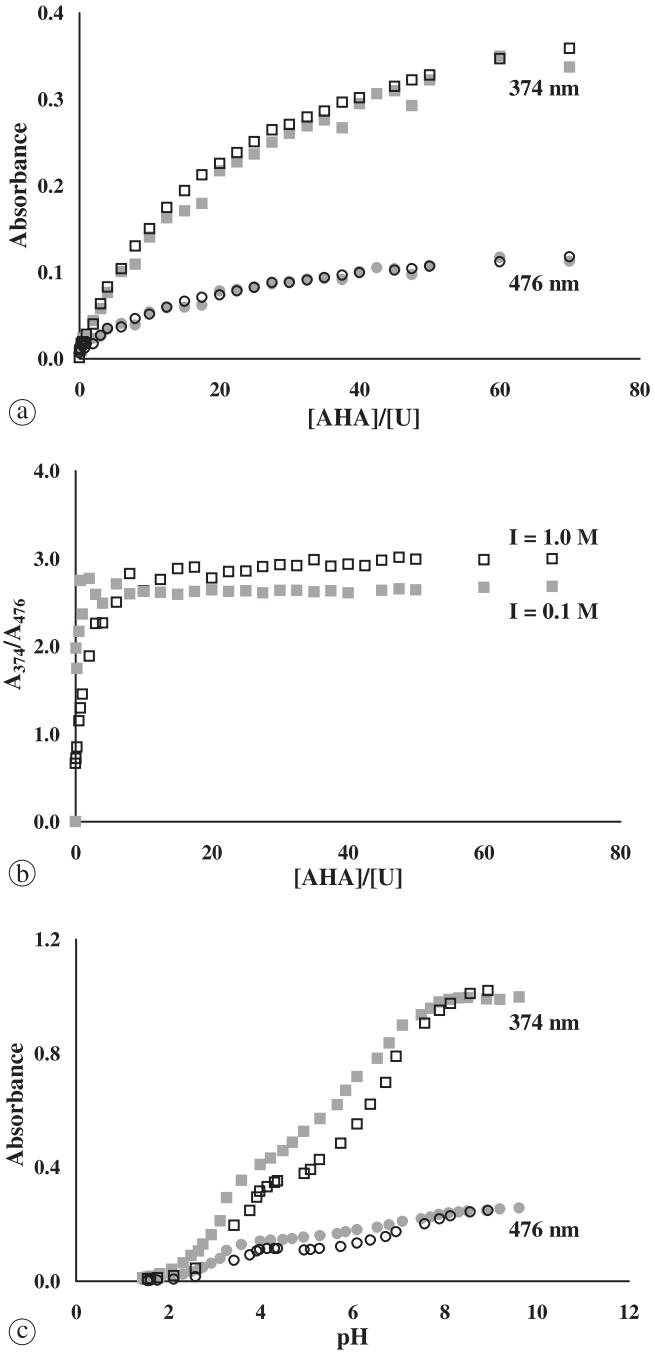

Fig. 3. (**a**) Effect of relative AHA concentration on the peak maxima of 1 mM U at pH 4.0. Closed, 0.1 M ionic strength; open, 1.0 M ionic strength. (**b**) Effect of the ionic strength on the relative maxima at pH 4.0. Closed, 0.1 M ionic strength; open, 1.0 M ionic strength. (**c**) Effect of pH titration on the absorbance of a 1 mM uranyl solution. Closed, 10 mM AHA; open, 20 mM AHA.

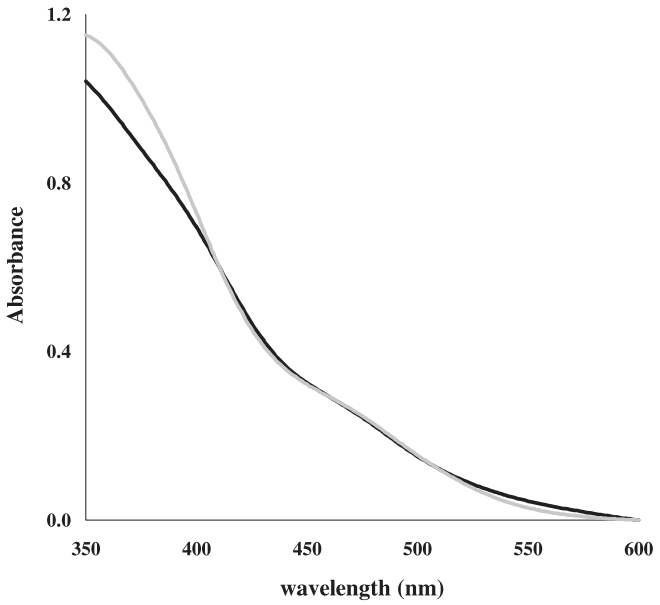

Fig. 4. Comparison of the absorbance of the solid in a KBr glass (gray) to an aqueous sample of 1 mM U, 10 mM AHA, 1.0 M ionic strength ($NaClO_4$), pH 8.1 (black); normalized at 476 nm.

ing ligand concentration. Fig. 3b shows that the ratio of the two maxima depends on ionic strength; at 0.1 M ionic strength, the spectra reach an equilibrium almost immediately (1 equivalent AHA), but at 1.0 M ionic strength, the equilibrium is not reached until more than 8 equivalents of AHA are added. Both maxima increase with increasing AHA concentration, but the absorbance at 374 nm, the larger maximum, is higher at the higher ionic strength, while the absorbance at 476 nm is the same. The effect was observed with both sodium nitrate and perchlorate. Fig. 3c demonstrates that as the pH is increased, the absorbance of a 1 mM uranyl solution reaches a maximum value independent of AHA concentration, indicating that the uranyl is fully complexed.

Fig. 4 demonstrates that the absorption spectrum of the solid complex in a transparent KBr glass closely resembles that of the high pH aqueous UAHA complex.

3.3.2 FT-IR

The IR spectra of the purified product and its deuterated analogue are presented in Fig. 5 and their assignments in Table 4. The spectra are normalized to the U=O peak. The product had incomplete H−D exchange after three dissolution/drying cycles, so the N−H stretch can still be seen. However, a strong N−D peak is seen at 2411 cm^{-1}, and the N−H rock at 1580 cm^{-1} disappears. FT-IR spectra of the UAc, AHA, and FeAHA have been reported previously [47, 64–68] and assignments are made accordingly. The spectra are similar to those of the $Fe(AHA)_3$ complex.

3.3.3 NMR

The aqueous UAHA ^{1}H NMR spectra, along with their corresponding UV-vis spectra, are presented in Fig. 6. Only the portions of the spectra with signal are presented. For comparison, the peaks of UAHA, FeAHA, and AHA in all the solvents studied are summed in Table 5. The assignments of the *E* and *Z* AHA isomers follow those in the literature [34], the UAHA O,O bidentate methyl peak is inferred by comparison to FeAHA, and the rest by relative integration. The aqueous spectra show only the methyl peaks of the UAHA and dissociated AHA; the N−H and O−H have exchanged. The two UAHA peaks cannot be resolved, so the mono- and bidentate UAHA complexes cannot be quantified, but the degree of dissociation can be determined. This method is being pursued in our laboratory to directly determine the uranyl-AHA aqueous stability constants. At low pH, we measure *via* relative integration that the UAHA complex is 88.7% dissociated, with 1.7% of the free ligand as *E*-isomer; this corresponds to literature. The UAHA is almost entirely the open-chain complex determined by EXAFS. An

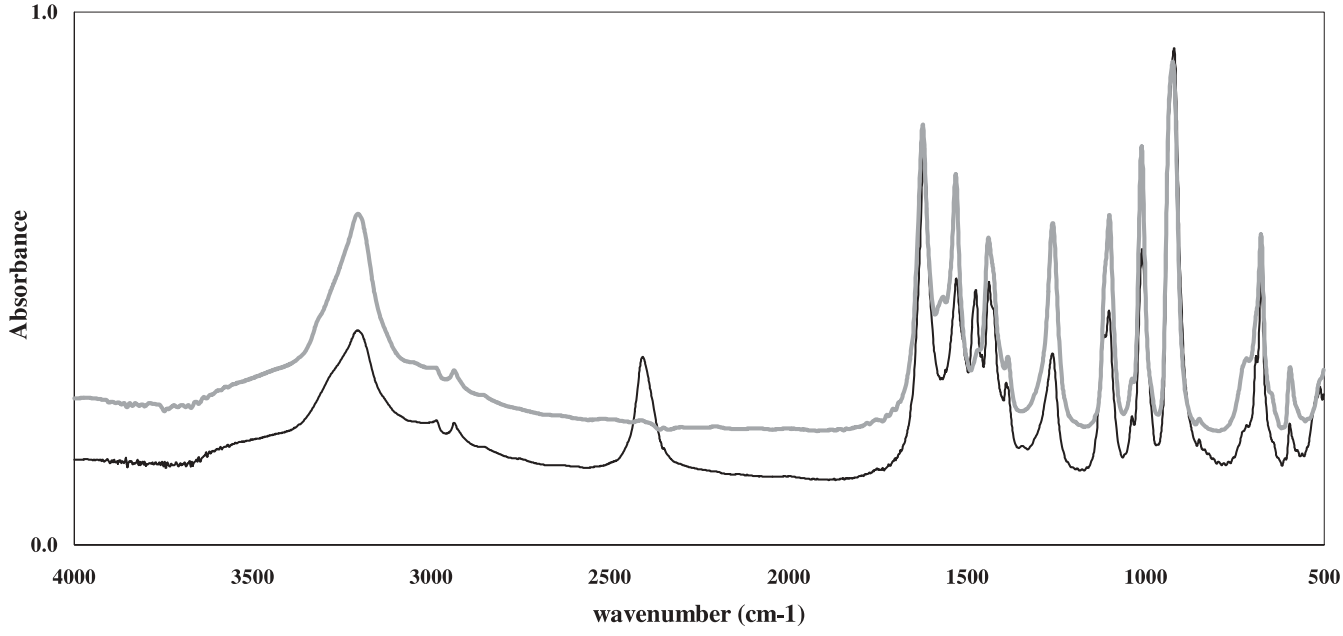

Fig. 5. FT-IR of the UAHA complex, before (black) and after (gray) D_2O exchange, normalized to the uranyl stretch.

Table 4. (**a**) Infrared peaks and assignments (cm^{-1}). (**b**) Infrared absorption peaks and assignments of deuterated compounds (cm^{-1}).

(**a**) UAc	AHA	UAHA	FeAHA	Assignment
3352				O−H stretch (from hydrate)
	3207	3209	3217	N−H stretch
	3212, 3055, 3011			O−H (intrabonded)
2975, 2924	2930, 2860	2984, 2935	2899, 2839	Alkyl C−H stretch
	2860	2839		Alkyl C−H stretch
	1644	1627	1595	C=O, C−N
1516	1560	1580, 1530	1523	C=O, N−H rock
1477	1455, 1449	1440	1442	CH_3 def.
1385	1380	1385	1387	CH_3 def.
	1321	1265	1331	N−H rock
	1090	1104	1084	N−O
1053	992		1043	CH_3 rock
1023	966	1010	993	CH_3 rock, C−C
945		925		UO_2 stretch
	750			
697	650	675	673	C=O def.

(**b**) AHA	UAHA	FeAHA	Assignment
3028, 2833	2985, 2936	3006, 2835	Alkyl C−H stretch
2376	2411	2290	N−D stretch
2150			O−D stretch
1663	1621	1610	C=O
1481	1473	1474	N−D bend
1443	1438	1434	CH_3 def.
1378	1386	1387	CH_3 def.
	1122	1133	N−O
1090	1104	841	N−D rock
1043	1042	1042	CH_3 rock
987	1009	994	CH_3 rock, C−C
	921		UO_2 stretch
679	675	673	C=O def.

upfield shoulder due to the bidentate UAHA is seen. At circumneutral pH, the peaks cannot be resolved, but a broad peak is seen upfield of the acidic methyl pH. Sharp peaks from free AHA (1.96 and 1.84 ppm) and residual acetone (2.08 ppm) overlap with the UAHA. Smaller peaks, possibly due to uranyl hydroxide, are also seen. At basic pH, uranyl would precipitate as the hydroxide, so excess AHA was added to solubilize the complex. This spectrum is com-

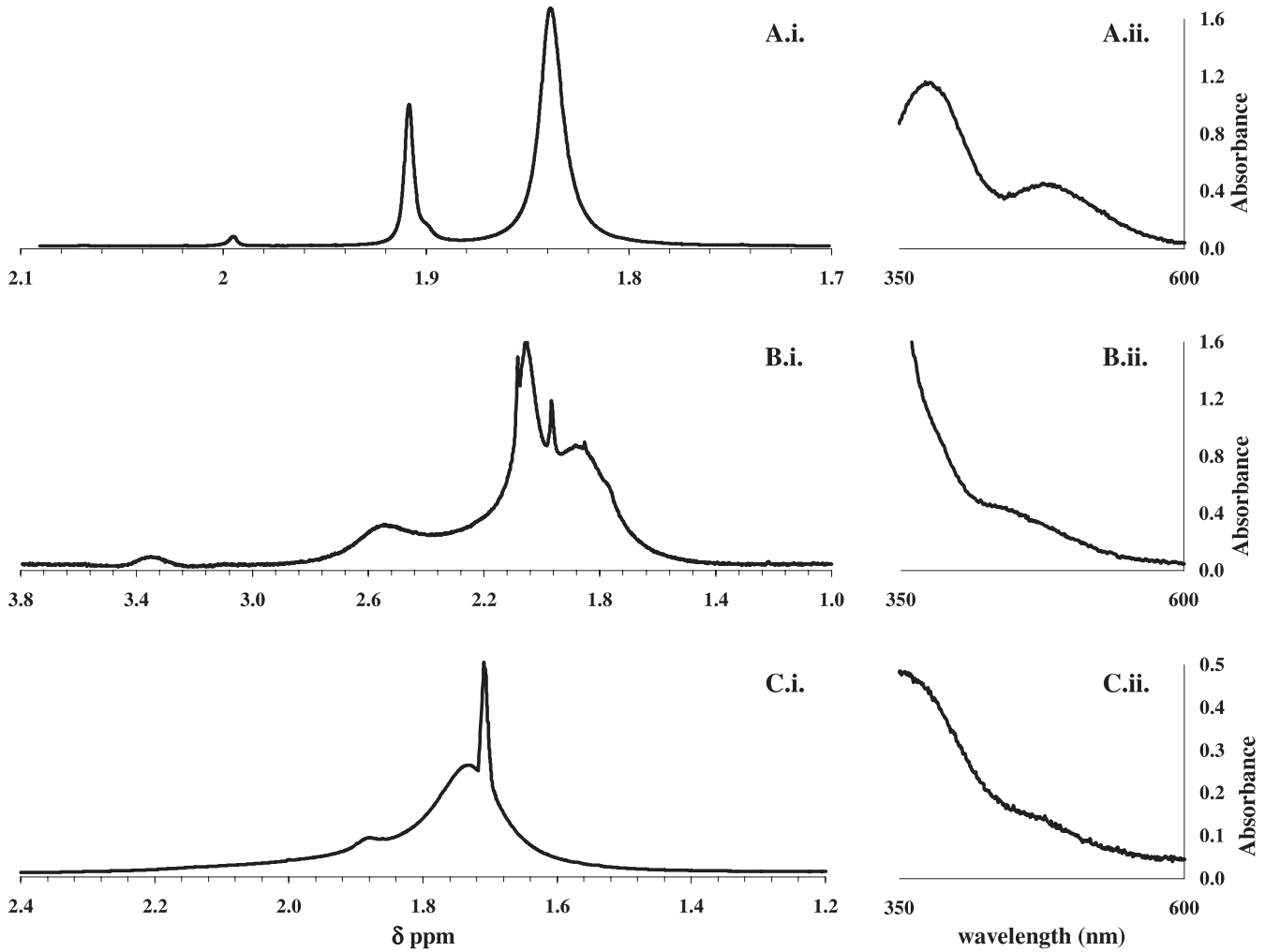

Fig. 6. Details of the aqueous NMR spectra of the UAHA complex. i. Region of interest in the NMR spectrum. ii. UV-vis spectra of the NMR solutions. (**a**) D_2O/DNO_3; (**b**) D_2O; (**c**) D_2O/NaOD, excess AHA.

posed of the two broad UAHA peaks at 1.72 and 1.85 ppm; the sharp peaks of the free AHA molecules are seen at 1.70 and 2.00 ppm. The UV-vis spectrum of this solution is identical to the spectra of uranyl with excess AHA above pH 8.0, seen in Fig. 2.

The methyl peak of UAHA in DMSO is identical to that of FeAHA, far downfield of free AHA. There is only one methyl peak, indicating that the solid UAHA has a single geometry of ligand binding. Unlike FeAHA in DMSO, however, the N−H peak does not have the expected relative integration to the methyl peak. This cause is unknown, as the N−H bond is clearly seen with FT-IR spectroscopy. The ferromagnetic effect broadens the peaks of the FeAHA complex; only a broad water peak is seen for the aqueous complex at circumneutral pH, and even the free methyl peak from dissociation at low pH is broadened.

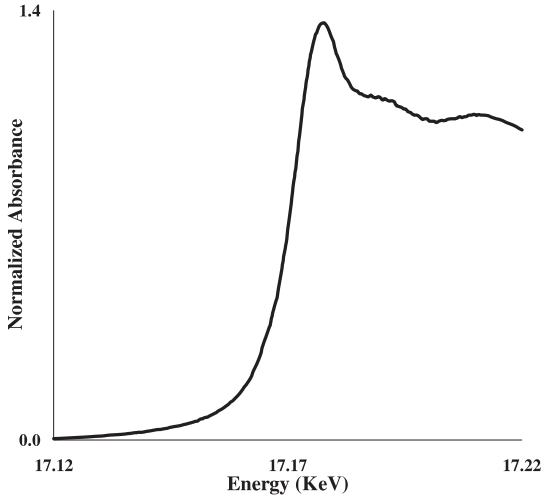

Fig. 7. XANES spectrum of the unpurified UAHA complex.

3.3.4 EXAFS

XANES analysis

As seen in Fig. 7, the position of the edge energy is consistent with U(VI). The presence of shoulder at 17.19 keV indicates that U(VI) is present as the UO_2^{2+} moiety. There is no indication of U(IV) from reduction of U(VI) by AHA.

EXAFS analysis

EXAFS spectra were extracted, k^2-weighted and Fourier transform performed between k [3, 14.75] Å^{-1}. The adjustments of EXAFS spectra were performed under the constraints $S_0^2 = 0.9$, a single value of energy shift ΔE_0 was

Table 5. NMR peaks and assignments[a].

Solvent	Sample	δ ppm[b] (Int.)[c], Assignment
DMSO	AHA	10.31 (18.07), *E* N−H; 9.76 (2.02), *Z* N−H; 9.09 (2.08), *Z* O−H; 8.65 (18.27), E O−H; 1.85 (6.43), *E* Me; 1.66 (53.13), *Z* Me
	FeAHA	7.23 (27.11), N−H; 3.33 (72.89), Me
	UAHA	3.32 (95.53), Me; 1.66 (4.43), N−H
D_2O	AHA	1.95 (4.20), *E* Me; 1.72 (95.80), *Z* Me
	FeAHA	4.51 (HOD, broadened)
	UAHA	2.08, residual acetone; 2.04 (broad), monodentate UAHA; 1.96 (sharp), free *E* AHA; 1.85 (broad), bidentate UAHA; 1.84 (sharp), free *Z* AHA
D_2O/DNO_3	AHA	1.78 (4.40), *E* Me; 1.61 (95.60), *Z* Me
	FeAHA	1.36 (100), free AHA Me
	UAHA	2.00 (1.34), free *E* AHA; 1.91 (21.30), monodentate UAHA; 1.89 (shoulder), bidentate UAHA; 1.84 (77.36), free *Z* AHA
$D_2O/NaOD$	AHA	1.72 (6.93), *E* Me; 1.61 (93.07), *Z* Me
	UAHA + AHA	2.00 (sharp), free *E* Me; 1.87 (broad), monodentate UAHA; 1.73 (broad), bidentate UAHA; 1.70 (sharp), free *Z* Me
CD_3CN	AHA	9.05 (17.16), *Z* N−H; 7.64 (18.29), *Z* O−H; 2.22 (3.32), *E* N−H, O−H; 1.99 (3.64), *E* Me; 1.80 (57.59), *Z* Me
CD_3CN/DNO_3	UAHA[d]	2.01 (5.19), free *E* AHA Me; 2.00 (74.21), UAHA Me; 1.88 (16.97), free *Z* AHA Me; 1.19 (3.64), UAHA N−H

a: Solvent peaks excluded;
b: Using solvent as internal reference;
c: Integration normalized to 100%;
d: The integrations do not correspond to expected geometry due to some N−H exchange with D_2O/DNO_3.

used for all scattering. The uncertainty on the coordination number (C.N) is 20%, the uncertainty on the distance (*R*) is 0.02 Å.

The following contributions were used for the fitting procedure:

- The single scattering U = O around 1.8 Å.
- The single scattering U−O(H_2O) corresponding to the O atoms of the H_2O molecule.
- The single scattering U−O(AHA) corresponding to the O atoms of the AHA group.
- The multi scattering U=O (MS) around 3.6 Å.
- The single scattering U−N around 3.4 Å.

Fitted Fourier transform and k^2-EXAFS spectra are shown in Figs. 8 and 9. The structural parameters are presented in Table 6.

EXAFS analysis indicates that the first coordination shell around the UO_2^{2+} moiety consists of 3.2 ± 0.6 water molecules and 1.7 ± 0.3 oxygen atoms from AHA. The second coordination sphere contains 2.1 ± 0.4 nitrogen atoms.

Chemical analysis indicates two AHA groups per uranyl moiety, and EXAFS indicates 1.7 ± 0.3 oxygen atoms from AHA in the first coordination sphere. In addition, there is no indication of U − U scattering; the complex is not polymeric. Since the two molecules supply only two oxygen atoms for each U atom, we conclude that the AHA is bonded to the UO_2^{2+} in a monodentate fashion in the unpurified EXAFS sample, which is slightly acidic. Representations of the structures of the complex are shown in Fig. 10; AHA and FeAHA are shown for comparison.

Table 6. EXAFS structural parameters for unpurified UAHA.

U-AHA		Structural parameter		
Scattering	C.N.	*R* (Å)	σ^2 (Å^2)	E_0 (eV)
U=O	1.8	1.78	0.0013	14.46
U−O(AHA)	1.7	2.33	0.0015	14.46
U−O(H_2O)	3.2	2.50	0.0025	14.46
U−N	2.1	3.43	0.0018	14.46
U=O(MS)	2	3.57	0.003	14.46
Residual		11.6%		

3.3.5 Laser fluorescence

The fluorescence spectra of the UAHA complex and AHA starting materials both matched background. The UAc starting material displayed its characteristic spectrum [67].

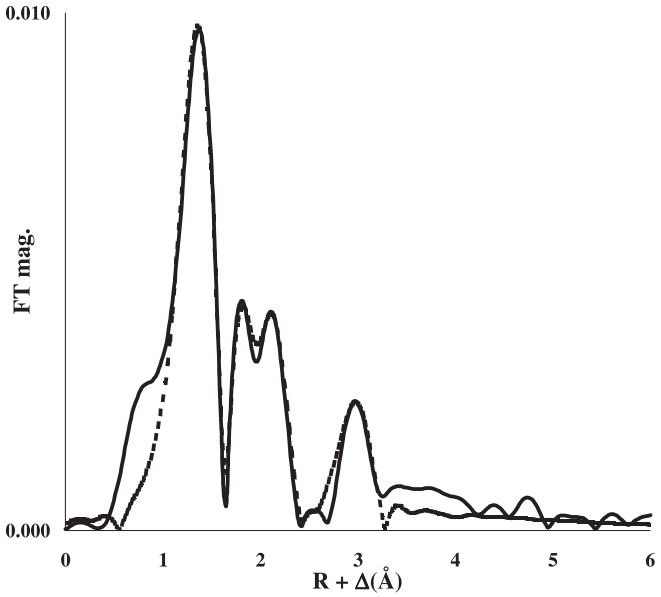

Fig. 8. Fitted Fourier transform of k^2-EXAFS spectra of U-AHA. Adjustment between $k = [3,\ 14.75]$ Å^{-1}. Solid line, data; dashed line, fit.

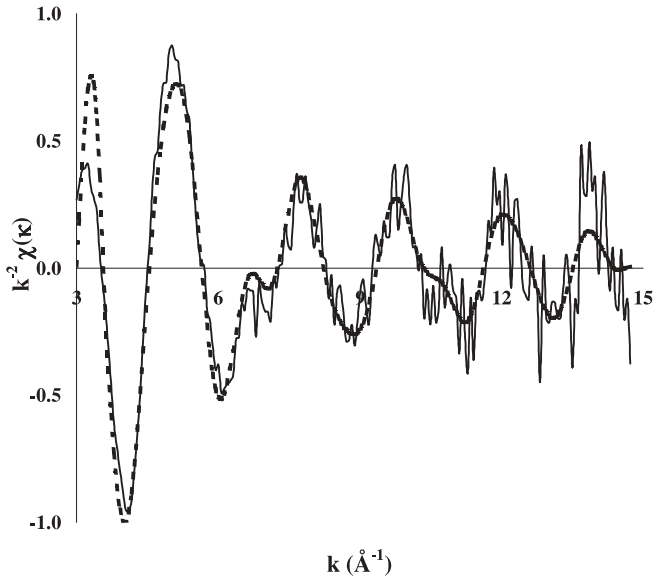

Fig. 9. Fitted k^2-EXAFS spectra of U-AHA. Adjustment between $k = [3,\ 14.75]$ Å^{-1}. Solid line, data; dashed line, fit.

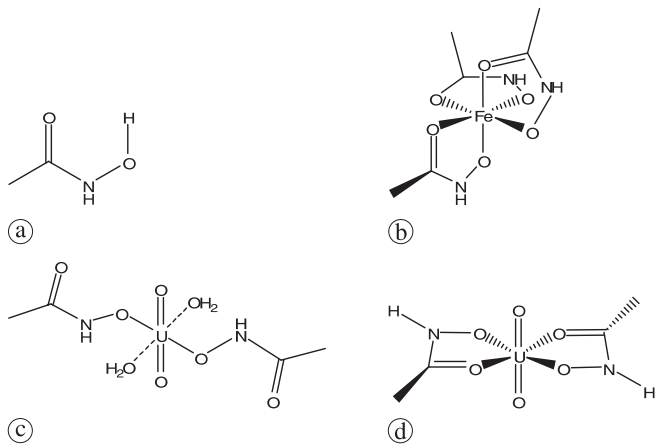

Fig. 10. (**a**) Structure of acetohydroxamic acid. (**b**) Structure of ferric-trisacetohydroxamate [21]; (**c**) Monodentate UAHA structure, present at low pH; (**d**) Bidentate UAHA structure.

4. Discussion

4.1 Synthesis and purification

The solid-state reaction is facile with mechanical or heat energy, and likely aided by the release of waters bound to the UAc and AHA starting materials. Mechanical grinding has the best results largely because the reaction can be monitored by the color and texture. In addition, the mild conditions discourage thermal breakdown of the AHA starting material and the hydrolysis of AHA and uranyl. Beginning with two molar equivalents of AHA is optimal: larger amounts are wasted and the additional material hinders grinding. The amount of starting material recovered decreases significantly as more AHA is added, indicating that the excess starting materials are simply washed away during the purification step. UAc is preferred over uranyl nitrate hexahydrate, though the latter forms UAHA more easily; uranyl nitrate releases more water and nitric acid as byproducts, making it more difficult to purify. The solubility of the starting materials in acetone – and the insolubility of the UAHA product – enables easy purification with an acetone wash. Attempts to form the solid from acetone precipitation were unsuccessful, indicating that unreacted starting materials are washed away, not dissolved and precipitated as UAHA.

4.2 Chemical characterization

The presumed $UO_2(AHA)_2$ stoichiometry of the product is confirmed by [U] and [AHA] assays. Its solubility in water is limited by its quick dissociation, and its aqueous UV-vis spectrum resembles that of sparingly soluble uranyl hydroxide. Acetone and acetonitrile will dissolve UAHA when acidified, but not when water alone is added. This is likely due to the different conformation in acidic media.

4.3 Spectroscopic characterization

The ^{1}H NMR spectrum in DMSO does not integrate cleanly but the FT-IR clearly shows an N−H peak. Its chemical shifts are similar to the known FeAHA, indicating that the solid UAHA is indeed described by Fig. 10d.

The UV-vis spectra depend on ionic strength (ratio of maxima), pH (peak shift), and amount of AHA (absorbance). A steady absorbance spectrum is attained with increasing pH, indicating complete complexation, but under acidic conditions the peaks shift and absorbance does not stabilize, even at thousandfold excess AHA concentrations, indicating that increasing pH does not simply lead to an increasing number of ligands. The spectral change is therefore likely due to a change in speciation. A comparison of the solid and solution UV-vis spectra indicate that the dominant aqueous complex in neutral and basic conditions is indeed a bidentate dihydroxamate UAHA, and not a mixed UAHA-hydroxide species. This is analogous to ferric, nickel, and lanthanum structures. The EXAFS, the pH-dependent shifts in UV-vis and NMR spectra, and the enhanced solubility in acidified solvents indicate a monodentate $UO_2(AHA)_n$ complex at low pH (Fig. 10c), where n depends on the relative concentration of AHA and can be greater than 2. This structure could be stabilized by intramolecular hydrogen

bonding, including between the yl oxygen atoms and the carbonyl oxygen of the AHA.

We demonstrate that at AHA binds uranyl with at least two geometries, which are by EXAFS, UV-vis, and FT-IR shown to be mono- and bidentate; the bidentate complex has a higher molar absorptivity and dominates the UV-vis spectrum, though the two complexes coexist, and a UV-vis basis set can be determined for the bidentate complex for use in modeling the uranyl-AHA interaction in the UREX complex.

5. Conclusions

The reported synthesis and purification method is a new, facile and high-yielding route to pure uranyl-AHA, and the analogous ferric-AHA compound can be prepared similarly. The insolubility of the complex in the examined nonpolar solvents is consistent with its nonextraction during UREX.

The FT-IR, UV-vis, EXAFS, and chemical characterizations of the solid confirm its identity. Solubility and solution-phase NMR studies in the absence of water and counterions are made possible with the solid; further studies of the formation constant can be performed with precise control.

The pH effects on the aqueous structure seen using aqueous ^{1}H-NMR correlate to changes in the UV-vis spectra. Two distinct moieties are present, and the distribution between the two is pH-dependent. The UV-vis of the solid matches basic solution-phase spectra; the aqueous UAHA compound can now be modeled with confidence at basic pH as bidentate $UO_2(AHA)_2$ with no hydroxide. The low-pH NMR shows a single conformation, corresponding to the UV-vis spectrum with maxima at 374 and 476 nm; EXAFS confirms the monodentate structure. Future modeling can now include the two binding moieties for increased accuracy.

The proposed bidentate structure of the solid is analogous to known ferric, nickel, and lanthanum complexes, and the spectroscopy correlates strongly to those of the known FeAHA complex. A crystal structure is being pursued for confirmation.

Acknowledgment. Nous voulons remercier tous les Thaka, et specialement Tom O'Thaka pour son aide concernant la radioprotection. The authors would like to acknowledge Nicholas A. Smith for his help with laser fluorescence. This work was supported by the US Department of Energy, agreement no. DE-FG07-01AL67358. Use of the Advanced Photon Source was supported by the U. S. Department of Energy, Office of Science, Office of Basic Energy Sciences, under Contract No. DE-AC02-06CH11357.

References

1. Laidler, J. J., Collins, E. D., Duguid, J., Henry, R. N., McDeavitt, S. M., Thompson, M., Toth, L. M., Williamson, M., Willit, J. L.: Preparation of a technology development roadmap for the accelerator transmutation of waste (ATW) system: Report of the ATW separations technologies and waste forms technical working group. Argonne National Laboratory Report, ANL-99/15 (1999).
2. Laidler, J. J.: Development of separations technologies in the US partitioning and transmutation programme. Presented at the Seventh Information Exchange Meeting on Actinide and Fission Product Partitioning and Transmutation, Jeju, Republic of Korea (2002).
3. Paiva, A. P., Malik, P.: Recent advances on the chemistry of solvent extraction applied to the reprocessing of spent nuclear fuels and radioactive wastes. J. Radioanal. Nucl. Chem. **261**(2), 485 (2004).
4. Taylor, R. J., May, I., Wallwork, A. L., Denniss, I. S., Hill, N. J., Galkin, B. Y., Zilberman, B. Y., Fedorov, Y. S.: The applications of formo- and aceto-hydroxamic acids in nuclear fuel reprocessing. J. Alloys Cmpd. **271**–**273**, 534 (1998).
5. May, I., Taylor, R. J., Brown, G.: The formation of hydrophilic Np(IV) complexes and their potential application in nuclear fuel reprocessing. J. Alloys Cmpd. **271**–**273**, 650 (1998).
6. Barocas, A., Baroncelli, F., Biondi, G. B., Grossi, G.: The complexing power of hydroxamic acids and its effect on behaviour of organic extractants in the reprocessing of irradiated fuels – II. The complexes between benzohydroxamic acid and thorium, uranium(IV) and plutonium(IV). J. Inorg. Nucl. Chem. **28**, 2961 (1966).
7. Chung, D. Y., Lee, E. H.: The reduction of Np(VI) by acetohydroxamic acid in nitric acid solution. Bull. Korean Chem. Soc. **26**(11), 1692 (2005).
8. Schroeder, N., Altrep, M.: Technetium and iodine separations in the UREX process. Advanced Fuel Cycle Initiative Report, LA-UR-01-6607 (2001).
9. Taylor, R. J., May, I.: The reduction of actinide ions by hydroxamic acids. Czech. J. Phys. **49**, 617 (1999).
10. Colston, B. J., Choppin, G. R., Taylor, R. J.: A preliminary study of the reduction of Np(VI) by formohydroxamic acid using stopped-flow near-infrared spectroscopy. Radiochim. Acta **88**, 329 (2000).
11. Advanced Accelerator Applications Report, AAA-PDO-GEN-01-0033 (2001), p. 5.
12. Advanced Fuel Cycle Initiative Report, LA-UR-02-2630 (2002), p. 45.
13. Sekhon, B. S., Kaur, N.: Complex formation equilibria of aceto-hydroxamic acid with H^+ and UO_2^{2+} ion in aqueous organic mixtures. J. Indian Chem. Soc. **72**(8), 545 (1995).
14. Koide, Y., Uchino, M., Shosenji, H., Yamada, K.: Studies of collectors. X. Complexing ability of amino hydroxamic acid ligands with dioxouranium(VI) in aqueous solution. Bull. Chem. Soc. Japan. **62**, 3714 (1989).
15. Czerwinski, K. R., Bowman, M., Plaue, J.: Complexation of lanthanides and actinides by siderophores. Paper presented at the 216th ACS National Meeting, Boston, August 23–27 (1998).
16. Neu, M. P., Matonic, J. H., Ruggiero, C. E., Scott, B. L.: Structural characterization of a plutonium(IV) siderophore complex: Single-crystal structure of Pu-desferrioxamine E. Angew. Chem. Int. Edit. **39**(8), 1443 (2000).
17. John, S. G., Ruggiero, C. E., Hersman, L. E., Tung, C.-S., Neu, M. P.: Siderophore mediated plutonium accumulation by *Microbacterium flavescens* (JG-9). Environ. Sci. Technol. **35**, 2942 (2001).
18. Brainard, J. R., Srietelmeier, B. A., Smith, P. H., Langston-Unkefer, P. J., Barr, M. E., Ruan, R. R.: Actinide binding and solubilization by microbial siderophores. Radiochim. Acta **58**–**59**(2), 357 (1992).
19. Bouby, M., Billard, I., MacCordick, J., Rossini, I.: Complexation of uranium VI with the siderophore pyoverdine. Radiochim. Acta **80**(2), 95, (1998).
20. Boukhalfa, H., Reilly, S. D., Smith, W. H., Neu, M. P.: EDTA and mixed-ligand complexes of tetravalent and trivalent plutonium. Inorg. Chem. **43**, 5816 (2004).
21. Failes, T. W., Hambley, T. W.: Crystal structures of tris(hydroxamato) complexes of iron(III). Aust. J. Chem. **53**, 897 (2000).
22. García, B., Ibeas, S., Muñoz, A., Leal, J. M.: NMR studies of phenylbenzohydroxamic acid and kinetics of complex formation with nickel(II). Inorg. Chem. **42**, 5434 (2003).
23. Brown, D. A., Glass, W. K., McGardle, S. J. C.: Monohydroxamic acid complexes of iron(II and III), cobalt(II and III), copper(II) and zinc(II). Inorg. Chem. Acta **80**, 13 (1983).
24. Rudzka, K., Arif, A. M., Berreau, L. M.: Chemistry of a Ni(II) acetohydroxamic acid complex: Formation, reactivity with water, and attempted preparation of zinc and cobalt analogues. Inorg. Chem. **44**, 7234 (2005).
25. Celina, M., Fernandes, M. M., Paniago, E. B., Carvalho, S.: Copper(II) mixed ligands complexes of hydroxamic acids with

glycine, histamine, and histidine. J. Braz. Chem. Soc. **8**(5), 537 (1997).
26. Biruš, M., van Eldik, R., Gabričević, M., Zahl, A.: ^{139}La NMR kinetic study of lanthanum(III) complexation with acetohydroxamic acid. Eur. J. Inorg. Chem. **2002**(4), 819 (2002).
27. Dominey, L. A., Kustin, K.: Kinetics and mechanism of iron(II), cobalt(II), and nickel(II) mono complex formation with acetohydroxamic acid. Inorg. Chem. **23**(1), 103 (1984).
28. Edwards, D. C., Myneni, S. C. B.: Near edge X-ray absorption fine structure spectroscopy of bacterial hydroxamate siderophores in aqueous solutions. J. Phys. Chem. A **110**, 11 908 (2006).
29. Edwards, D. C., Myneni, S. C. B.: Hard and soft X-ray absorption spectroscopic investigation of aqueous Fe(III)-hydroxamate siderophore complexes. J. Phys. Chem. A **109**, 10 250 (2005).
30. Boukhalfa, H., Reilly, S. D., Michalczyk, R., Iyer, S., Neu, M. P.: Iron(III) coordination properties of a pyoverdin sideophore produced by Pseudomonas putida ATCC 33015. Inorg. Chem. **45**, 5607 (2006).
31. Gong, C. S., Sullens, T. A., Daniels, J., Czerwinski, K. R.: Use of dyes for spectroscopic uranyl speciation determination. Paper presented at the 232nd ACS National Meeting, San Francisco, CA, United States, Sept. 10–14 (2006).
32. Sinkov, S. I., Choppin, G. R., Taylor, R. J.: Complexation and redox chemistry of U(VI) , Np(V) and Pu(VI) with acetohydroxamic acid. Paper presented at the 232nd ACS National Meeting, San Francisco, CA, United States, Sept. 10–14 (2006).
33. Brown, D. A., Glass, W. K., Mageswaran, R., Girmay, B.: Cis-trans isomerism in monoalkylhydroxamic acids by ^{1}H, ^{13}C, and ^{15}N NMR spectroscopy. Magn. Reson. Chem. **26**, 970 (1988).
34. Senent, M. L., Niño, A., Muñoz-Caro, C., Ibeas, S., García, B., Leal, J. M., Secco, F., Venturini, M.: Deprotonation sites of acetohydroxamic acid isomer s. A theoretical and experimental study. J. Org. Chem. **68**, 6535 (2003).
35. Kaczor, A., Proniewicz, L. M.: The structural study of acetohydroxamic and oxalodihydroxamic acids in DMSO solution based on the DFT calculations of NMR spectra. J. Mol. Struct. **704**, 189 (2004).
36. Brown, D. A., Glass, W. K., Mageswaran, R., Ali Mohammed, S.: ^{1}H and ^{13}C NMR studies of isomerism in hydroxamic acids. Magn. Reson. Chem. **29**, 40 (1991).
37. El Yazal, J., Pang, Y.-P.: Novel stable configurations and tautomers of the neutral and deprotonated hydroxamic acids predicted from high-level ab inition calculations. J. Phys. Chem. A **103**, 8346 (1999).
38. Kakkar, R., Grover, R., Chadha, P.: Conformational behavior of some hydroxamic acids. Org. Biomol. Chem., **1**, 2200 (2003).
39. Cross, J. B., Duca, J. S., Kaminski, J. J., Madison, V. S.: The active site of a zinc-dependent metalloproteinase influences the computed pK_a of ligands coordinated to the catalytic zinc ion. J. Am. Chem. Soc. **124**(37), 11 005 (2002).
40. Wirgau, J. I., Spasojević, I., Boukhalfa, H., Batinić-Haberle, I., Crumbliss, A. L.: Thermodynamics, kinetics, and mechanism of the stepwise dissociation and formation of tris(l-lysinehydroxamato)iron(III) in aqueous acid. Inorg. Chem. **41**, 1464 (2002).
41. Ventura, O. N., Rama, J. B., Turi, L., Dannenberg, J. J.: Acidity of hydroxamic acids: An ab initio and semiempirical study. J. Am. Chem. Soc. **115**, 5754 (1993).
42. Agrawal, Y. K., Khare, V. P., Kapoor, A. S.: Thermodynamic ionization constants of hydroxamic acids. J. Electroanal. Chem. Interf. **54**, 433 (1974).
43. Eid Fazary, A.: Thermodynamic studies on the protonation equilibria of some hydroxamic acids in $NaNO_3$ solutions in water and in mixtures of water and dioxane. J. Chem. Eng. Data **50**, 888 (2005).
44. Poth Brink, C., Crumbliss, A. L.: Temperature-dependent acid dissociation constants (K_a, ΔH_a, ΔS_a) for a series of nitrogen-substituted hydroxamic acids in aqueous solution. J. Org. Chem. **47**, 1171 (1982).
45. Muñoz-Caro, C., Niño, A.: Modeling of protonation processes in acetohydroxamic acid. J. Org. Chem. **65**, 405 (2000).
46. Bagno, A., Comuzzi, C., Scorrano, G.: The site of ionization of hydroxamic acids probed by heteronuclear NMR relaxation rate and NOE measurements. An experimental and theoretical study. J. Am. Chem. Soc. **116**, 916 (1994).
47. Edwards, D. C., Nielsen, S. B., Jarzęcki, A. A., Spiro, T. G., Myneni, S. C. B.: Experimental and theoretical vibrational spectroscopy studies of acetohydroxamic acid and desferrioxamine B in aqueous solution: Effects of pH and iron complexation. Geochim. Cosmochim. Acta **69**(13), 3237 (2005).
48. Grenthe, I., Fuger, J., Konings, R. J. M., Lemire, R. J., Muller, A. B., Nguyen-Trung, C., Wanner, H.: *Chemical Thermodynamics of Uranium*. North-Holland Elsevier Science Publishers, Amsterdam (1992), vol. 1, p. 268.
49. Jiang, J., Rao, L., Di Bernardo, P., Zanonato, P., Bismondo, A.: Complexation of uranium(VI) with acetate at variable temperatures. J. Chem. Soc. Dalton Trans. **8**, 1832 (2002).
50. Matthews, R. B., Laidler, J.: Separations technology. Advanced Fuel Cycle Initiative Report, LA-UR-01-4283 (2001).
51. Karraker, D. G.: Radiation chemistry ot acetohydroxamic acid in the UREX process. Westinghouse Savannah River Company Report, WSRC-TR-2002-00282 (2002).
52. Laidler, J.: Separations technology. Advanced Fuel Cycle Initiative Report, LA-UR-02-0724 (2001).
53. Caceci, M. S., Choppin, G. R.: The first hydrolysis constant of uranium(VI). Radiochim. Acta **33**, 207 (1983).
54. Choppin, G. R., Mathur, J. N.: Hydrolysis of actinyl(VI) cations. Radiochim. Acta **52**/**53**, 25 (1991).
55. Jensen, M. P., Choppin, G. R.: Complexation of uranyl(VI) by aqueous orthosilicic acid. Radiochim. Acta **82**, 83 (1998).
56. Brown, P. L.: The hydrolysis of uranium(VI). Radiochim. Acta **90**, 589 (2002).
57. Stookey, L. L.: Ferrozine – a new spectrophotometric reagent for iron. Anal. Chem. **42**, 779 (1970).
58. Ueno, K., Imamura, T., Cheng, K. L.: *Handbook of Analytical Reagents*. CRC Press, Boca Raton, FL (1992), p. 189.
59. Ball, J. W., Nordstrom, D. K., McCleskey, R. B., To, T. B.: A new method for the direct determination of dissolved Fe(III) concentration in acid mine waters. Water-Resources Investigations Report, United States Geological Survey 99-4018A (1999), p. 297.
60. Hadži, D., Prevorëek, D.: Infra-red absorption bands associated with the NH group-III: Hydroxamic acids and derivatives. Spectrochim. Acta **10**, 38 (1957).
61. Carlon, H. R.: Quantitative liquid-phase infrared spectra of several simple organic compounds. Appl. Opt. **11**, 549 (1972).
62. Yanachkova, I. M., Staevsky, M.: Thermal decomposition of uranyl acetate. J. Mater. Sci. **8**, 606 (1973).
63. Kobayashi, I.: Thermal decomposition and air oxidation of some uranium compounds. Rikagaku Kenkyusho Hokoku **36**, 710 (1960).
64. Caldow, G. L., Van Cleave, A. B., Eager, R. L.: The infrared spectra of some uranyl compounds. Can. J. Chem. **38**, 772 (1960).
65. Volod'ko, L. V., Komyak, A. I., Sleptsov, L. E.: Infrared absorption spectrum of the sodium uranyl acetate single crystal. Zh. Prikl. Spec. **3**(1), 65 (1965).
66. Sałdyka, M., Mielke, Z.: Dimerization of the keto tautomer of acetohydroxamic acid-infrared matrix isolation and theoretical study. Spectrochim. Acta A **61**(7), 1491 (2005).
67. Sałdyka, M., Mielke, Z.: Infrared matrix isolation studies and ab inito calculations of acetohydroxamic acid. Pol. J. Chem. **77**, 1587 (2003).
68. Barabas, L., Gorguinpour, C., Leung, A. F., McCoy, J.: Spectroscopic measurements of temperature with uranyl compounds. Appl. Spec. **55**(10), 1382 (2001).